Reaction Pathways to Soot Formation in Petrodiesel and Biodiesel Combustion

G. Cai[1, *] and J. Abraham[1,2]
[1]School of Mechanical Engineering, University of Adelaide, North Terrace, SA 5005, Australia
[2]School of Mechanical Engineering, Purdue University, West Lafayette, Indiana, USA

Abstract

In this study, simulations are employed to improve the fundamental understanding of soot formation from a chemical kinetics perspective during biodiesel and petrodiesel combustion under pressure and temperature conditions in engines. n-Heptane is used as the surrogate for petrodiesel and a ternary mixture of methyl decanoate, methyl-9-decenoate, and n-heptane as the surrogate for biodiesel. In the case of the ternary biodiesel surrogate, a 211-species reduced mechanism is employed to model the chemical kinetics. This mechanism was derived as part of this work by combining reactions from the 160-species n-heptane mechanism with reactions from a skeletal 115-species mechanism proposed in the literature. Soot kinetics is represented using a chemical mechanism that models the growth of soot precursors starting from a single aromatic ring by hydrogen abstraction and carbon (acetylene) addition. The influence of turbulence is indirectly modelled through an imposed strain rate in the simulations. The computations are carried out using a strained laminar flamelet code (SLFC). Analysis of the results shows that the significant reduction in soot observed in biodiesel combustion results from an increase in the concentration of alkoxy species during the fuel breakdown process which, in turn, reduces the concentration of the aromatic species and the increased oxidation of the precursors that lead to the formation of the aromatic ring.

Keywords: Biodiesel combustion, Soot formation, Reaction pathway analysis, Strained flamelets

1. Introduction

In the diesel engine, fuel is injected directly into the cylinder toward the end of the compression stroke and it autoignites [1]. Combustion primarily occurs in a a highly strained and wrinkled diffusion flame surrounding the diesel jet and located where the fuel/air mixture is stoichiometric. Soot precursors form in the rich mixture fraction near the flame lift-off height where they become polycyclic aromatic hydrocarbons (PAHs) and eventually form soot downstream [2, 3]. In this work, through the use of kinetic modelling, a reaction pathway to soot formation is identified for petrodiesel and biodiesel combustion. This work is motivated by the desire to develop simple kinetic mechanisms for soot formation which can then be employed in multidimensional engine models and in large-eddy simulations. Understanding the reaction pathways and identifying the critical species will aid in the development of such models.

The turbulent diffusion flame surrounding the jet can be considered to be a collection of laminar flamelets [4,5]. In this work the unsteady laminar flamelet model will be employed to study the structure of the strained diffusion flamelets. The unsteady flamelet equation is given by

$$\frac{\partial \phi}{\partial t} = \frac{\chi}{2}\frac{\partial^2 \phi}{\partial Z^2} + \dot{\omega}_\phi \ , \qquad (1)$$

where χ is the scalar dissipation rate, ϕ denotes the vector of species mass fraction or temperature, and $\dot{\omega}_\phi$ represents their respective source terms. χ is defined as

$$\chi = 2D_Z(\nabla Z)^2 \ , \qquad (2)$$

where Z is the mixture fraction and D_Z is the molecular diffusivity of Z. In mixing layers, χ may be assumed to be related to Z by an error function profile [14]

$$\chi = \chi_{st} \frac{exp\left\{-2\left[erfc^{-1}(2Z)\right]^2\right\}}{exp\{-2[erfc^{-1}(2Z_{st})]^2\}} , \qquad (3)$$

where χ_{st} and Z_{st} represent the scalar dissipation rate and mixture fraction at the stoichiometric value, respectively. The next section will discuss the computational model and conditions that are employed for the analysis. Results and analysis will follow. The paper will close with summary and conclusions.

2. Computational Model

As petrodiesel consists of over 100 hydrocarbons, the direct chemical kinetic modelling of petrodiesel is computationally intensive even if kinetic mechanisms were completely available [6]. The fact is that such mechanisms are not yet available. For this study, n-heptane (C_7H_{16}) is used as the surrogate for petrodiesel as it has been shown to represent some aspects of the chemical kinetics of petrodiesel reasonably well [7,8]. A 160-species n-heptane surrogate mechanism was chosen [9] as it allowed for the best compromise between computational time and accuracy. In addition, the 160-species mechanism has sufficient detail for coupling with the soot mechanism.

Though the composition of biodiesel is simpler than of petrodiesel [10], the detailed oxidation kinetics of biodiesel is not well established. For this research, a ternary biodiesel surrogate fuel (TBS) is used. The TBS

* Corresponding author:
Phone: (+61) 08 8313 1120
Email: gary.cai@adelaide.edu.au

consists of three fuel components: 25% methyl decanoate (MD), 25% methyl-9-decenoate (MD9D) and 50% n-heptane. The TBS mechanism, developed as part of this work, is a 211-species mechanism which combines a 115-species skeletal TBS mechanism [11] with additional reactions from the 160-species n-heptane mechanism that influence soot kinetics. The additional reactions from the 160-species mechanism are those which also appear in a detailed oxidation model for methyl decanoate.

Soot is modelled using a 101-species, 546-reactions kinetic mechanism [12], which will be referred to as the ABF (Appel, Bockhorn, Frenklach) model. Soot formation involves several steps: inception of soot nuclei, surface growth, coagulation, and oxidation. The inception stage begins the pathway towards the formation of soot via specific precursors. Although the specific steps in the inception stage are not well-known, the pathway via PAHs is the most widely accepted. The PAH formation pathway forms soot though the H-abstraction-C2H2-addition (HACA) process [13,14]. Hydrogen atom is abstracted from a single aromatic ring (benzene) through collision with another molecule. The benzene ring (now a radical) reacts with acetylene (C2H2) to form the first chain.This is repeated until the single benzene ring (A1) becomes a naphthalene (A2) compound, and process is repeated. The aromatic rings then reach a stage where they are large enough to grow by surface growth and form particles. Large aromatic rings chemically bond to form larger structures, while the smaller PAHs continue growing through the inception stage. As the structures increases in size, they also agglomerate forming a range of structures. Throughout the stages of particle growth, oxidation of the soot, primarily via OH attack on the surface, works to reduce and limit soot inception and growth. In SLFC, soot formation is modelled by using the method of moments [15].

The NO mechanism from the GRI-Mech 3.0 is employed [16]. These three mechanisms (fuel, soot, and NO), added together, form the 253-species, 2085-reactions n-heptane mechanism and the 304-species, 1609-reactions TBS mechanism.

The unsteady flamelet equations (see Eq. (1)) are solved using an in-house strained laminar flamelet code (SLFC) to compute strained diffusion flames under engine conditions [17,18]. Note that the model includes the time derivative of pressure in the energy equation but the pressure is assumed to be constant in this work. SLFC models a laminar diffusion flamelet by transforming the physical space into Z space which is then discretized into 51 grid points. Note that it is this transformation which gives rise to the scalar dissipation rate in the equation. In this sense, the scalar dissipation rate is a measure of (square of) the physical gradients of the mixture fraction. The 51 grid points vary in density, with the highest density of the grid points close to Z_{st}.

The computations are carried out at a pressure of 42 bar. Fuel and air are initially at 373 and 1000 K, respectively. In addition, air is taken to be of atmospheric composition, with 21% oxygen by volume and the remainder nitrogen. The simulations are run for a total calculation time of 3 ms with a timestep of 5×10^{-7} s. It has been confirmed that this timestep is adequate to give timestep-independent results [8, 18-19].

3. Results and Discussion

3.1 Combustion Characteristics

For reference, the ignition delay time is found to be 0.42 ms for the n-heptane mechanism and 0.52 ms for the TBS mechanism. This is defined as the time where the peak temperature reaches 1,500 K. It is interesting to note that biodiesel ignition delay time is generally lower than that of petrodiesel. So, the results presented here are specific to the surrogate fuels selected and not a reflection of actual engine behaviour. Typical results from the computations are shown in Fig. 1 for n-heptane and TBS at 1.5 ms after ignition.

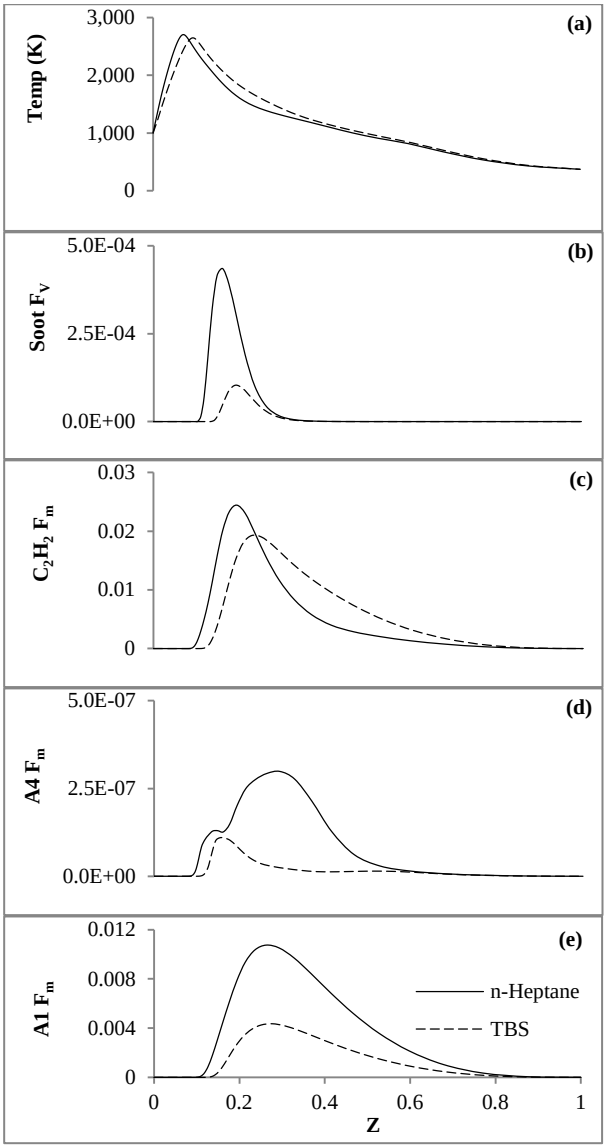

Figure 1: Plots for temperature, soot volume fraction, and acetylene, A4 and A1 mass fraction.

Temperature, soot volume fraction (f_v), and mass fractions (f_m) of, acetylene, A4, and A1 are shown with respect to Z. From the temperature plot (a), it can be seen that the peak temperature is similar between n-heptane and TBS although the Z where the peak occurs is different because Z_{st} is higher for biodiesel. These results are consistent with previous findings [19]. However, the soot f_v are lower in TBS by about a factor of four (Fig. 1(b)). This paper seeks to understand these differences from a kinetics perspective in the context of engine conditions. Recall that the soot mechanism used in this study is identical between the n-heptane and TBS mechanism, and that the HACA mechanism begins with the benzene (A1) species, subsequently forming A2, A3 and A4 through H-abstraction and C_2H_2-addition. In this regard, it is useful to compare the concentration of C_2H_2, A1, and A4 between n-heptane and TBS to identify differences. The difference in C_2H_2 concentration (Fig. 1(c)) of about 20% is not enough to explain the differences in soot. Comparing Fig. 1(d), it can be seen that the difference in A4 is in fact of the same magnitude as the difference in soot volume fraction. Fig. 1(e) shows that, while differences in A1 are not as large as in the soot f_v or A4 f_m, they are about a factor of three. The next section will discuss the origin of this difference.

3.2 Reaction Pathway Analysis

To understand the difference in A1 (and eventually, soot) between n-heptane and TBS, an understanding of the reaction pathway leading to the formation of A1 is needed. By tracing the formation of A1 through the various reactions that form it, critical species and reactions may be identified that cause this eventual difference. As the maximum f_m of A1 occurs at Z = 0.263 in n-heptane and Z = 0.277 for TBS, the pathway will be investigated at that Z for each surrogate fuel. Note that in terms of equivalence ratio, these Z correspond to 5.31 and 4.41, respectively, i.e. the peak A1 occurs at an overall leaner equivalence ratio in TBS than in n-heptane.

Table 1 shows the overall reaction pathway for the formation of A1 through its various precursors. The first column shows the reaction number. The next four columns list the chemical reaction and the Arrhenius reaction rate constants: the pre-exponential factor (A), the temperature-exponent (b), and the activation energy (E_A). For each reaction, a critical species is in **bold**. This species is identified as such because among the species at that level, it is most likely to influence the formation of A1. The species is investigated for its influence on the formation of soot. The last 3 columns list the mass fraction f_m of the critical species in n-heptane, TBS, and their ratio, respectively.

At the top level, reaction (henceforth, written as 'Rxn') 1.1 – 1.3 form A1. Comparing the ratios of the critical species, the ratios of n-C_4H_5 and n-C_6H_7 f_m are the largest which may explain the difference in A1 between n-heptane and TBS. However, the f_m of n-C_6H_7 is relatively low to cause such an impact in A1. Hence, Rxn 1.2 is the most likely route to A1. This type of evaluation is repeated to determine the key reactions and species that form n-C_4H_5. n-C_4H_5 is formed by numerous reactions, but only four important ones will be listed in Table 1. Comparing the ratios of species, it can be seen that the ratio of C_2H_3 f_m is largest between n-heptane and TBS. It is interesting to examine Rxn 2.3; the f_m of C_5H_5O is 125 times higher in TBS compared to n-heptane presumably because TBS is oxygenated.

Knowing the critical reaction and species in the 2nd level, the pathway can be traced back further to the 3rd. Only three of the numerous reactions are listed. Rxn 3.2 has a pre-exponential factor that is too low for the forward-direction reaction to affect A1 production. However, Rxn 3.2 is interesting due to the involvement of O_2 and HO_2. Although the forward reaction is very slow, it indicates that the reverse reaction is preferred. As HO_2 is almost 60,000 times more abundant in TBS than n-heptane at the peak A1 mixture fraction, this suggests that Rxn 3.2 is a very fast oxidising reaction that drastically slows down the formation of A1 in TBS by consuming C_2H_3. Comparing Rxn 3.1 and Rxn 3.3, although the former has a greater chance of forming C_2H_3, the critical species, IC_3H_7, is more abundant in n-heptane than TBS. Thus, reaction Rxn 3.3 is the most likely reaction that contributes to the difference in A1 at this level.

Table 1: Reaction pathway analysis for the formation of A1

1.1	**C_3H_3** + C_3H_3 = *A1*	2.0E+12	0	0	1.07E-04	9.51E-05	1.13
1.2	**n-C_4H_5** + C_2H_2 = *A1* + H	1.6E+18	-1.9	7400	3.64E-06	1.54E-07	23.6
1.3	**n-C_6H_7** = *A1* + H	5.3E+25	-4.4	17300	4.19E-09	9.61E-11	43.6
2.1	**C_2H_3** + C_2H_2 = *n-C_4H_5*	8.1E+37	-8.1	13400	5.19E-05	6.37E-06	8.15
2.2	**C_4H_6** + OH = *n-C_4H_5* + H_2O	6.2E+06	2	3430	1.72E-03	1.84E-03	0.935
2.3	**C_5H_5O** = *n-C_4H_5* + CO	2.5E+11	0	43900	1.43E-09	1.79E-07	7.99E-03
2.4	**C_5H_4OH** + O = CO_2 + *n-C_4H_5*	3.0E+13	0	0	5.99E-08	2.63E-08	2.28
3.1	**C_2H_4** (+M) = *C_2H_3* + H (+M)	1.69E+15	0.1	107099	5.16E-02	3.64E-02	1.42
3.2	C_2H_2 + **HO_2** = *C_2H_3* + O_2	2.73E-16	-0.9	11400	9.30E-13	5.33E-08	1.74E-05
3.3	C_2H_4 + **IC_3H_7** = *C_2H_3* + C_3H_8	1.31E+11	0	17800	1.29E-04	3.44E-07	375
4.1	H + **C_3H_6** = *IC_3H_7*	1.30E+13	0	1560	1.01E-02	3.99E-03	2.53
4.2	**C_3H_8** + O_2 = *IC_3H_7* + HO_2	4.00E+13	0	47500	5.98E-03	5.53E-05	108
4.3	H + **C_3H_8** = H_2 + *IC_3H_7*	1.30E+06	2.4	4471			
4.4	**CH_3** + C_3H_8 = CH_4 + *IC_3H_7*	3.98E+11	0	9500	1.33E-04	3.24E-05	4.10

The final level looks into the formation of IC_3H_7. Though there are many reactions that form IC_3H_7, only four reactions will be compared here. Looking at the hydrocarbon species, C_3H_8 has a much larger mass fraction in n-heptane than TBS and Rxn 4.2 can be concluded to form part of the critical pathway. Figure 2 summarizes the pathway identified above. For each species in the sequence, the f_m is significantly lower in TBS than n-heptane. It has been found that the pool of smaller hydrocarbons, such as C_2H_5, C_2H_6, and C_3H_8, has a smaller f_m in TBS than n-heptane by about 50%. The oxidation process of the biofuel does not easily disassociate the attached oxygen atoms due to the strong bonding force. The oxidation process of TBS initially breaks the fuel into more alkoxy groups, such as aldehyde and alcohol compared to n-heptane. A comparison of aldehydes and alcohols shows that their f_m in TBS is 60% higher than in n-heptane. The higher amount of oxygenated species reduces the proportion of hydrocarbons that are available to form soot precursors. While the focus in Table 1 is on C_3H_8, it has been replaced by C_mH_n in Fig. 2 to represent the collective pool of small hydrocarbons. This suggests that differences in the breakdown mechanism of TBS to these lower order hydrocarbons compared to that of n-heptane plays an important role in determining the final outcome.

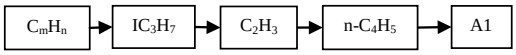

Another possible factor for the lower f_m of A1 in TBS is that it peaks at a leaner equivalence ratio: 4.41 as compared to 5.31 in n-heptane. Under leaner conditions, the amount of oxygen would naturally be higher, which in turn increases the oxidation of precursors of A1 and A1 itself. In fact, at the Z of peak A1, the O_2 concentration, while small, is still about six orders of magnitude larger in TBS than n-heptane. Its strong presence in TBS contributes significantly to the overall oxidation process through the creation of radicals such as O and OH. Referring back to Rxn 3.2 in Table 1, the high level of O_2 suggests that C_2H_3 can be more readily oxidised in the reverse reaction, thus also reducing the formation of soot.

Exhaust gas recirculation (EGR), the process of injecting a fraction of the exhaust gas back into the injection stream, has mostly been used to reduce NO_x at the expense of engine efficiency and an increase in particulates [1]. As it has been shown that the amount of O_2 strongly influences the formation of soot, an investigation into various EGR conditions has been carried out. It has been found that varying the initial O_2:N_2 ratio to reflect 20%, 40% and 60% EGR does not affect the conclusions arrived in this study. The detailed results will be discussed in a separate paper. A future paper will also discuss the development and validation of simplified mechanisms for biodiesel and petrodiesel soot kinetics with applications to engines.

4. Summary and Conclusions

In this study, an in-house laminar flamelet code was used to simulate the combustion of petrodiesel and biodiesel surrogates under engine conditions. n-Heptane was used as the surrogate for petrodiesel fuel and a ternary mixture of fuels was the surrogate for biodiesel fuel. It was found that the maximum concentration of soot volume fraction in n-heptane was larger than the surrogate biodiesel fuel by a factor of four. This difference is attributed to the difference in the initial aromatic species that leads to the formation of PAHs through the hydrogen-abstraction carbon-addition mechanism. This, in turn, is related to the higher concentration of alkoxy species formed during the oxidation of the biodiesel surrogate which, in turn, reduces the concentration of the hydrocarbon species that form the aromatic ring. Furthermore, the leaner mixture conditions under which the aromatic ring forms in the biodiesel surrogate contributes to the oxidation of the hydrocarbon species. This study suggests that simplified mechanisms for soot formation based on considering classes of species can be developed for more intensive CFD applications.

Acknowledgements

The authors thank Professor Bassam Dally and Dr. Zhao Tian for their feedback on this work. They also thank the School of Mechanical Engineering at the University of Adelaide and eResearch SA for providing access to computational resources.

References

[1] J.B. Heywood, Internal Combustion Engine Fundamentals, McGraw-Hill New York, US, 1988
[2] J. Dec, Proc. Comb. Inst. **32** (2009) 2727-2742
[3] C.K. Westbrook, Proc. Comb. Inst. **28** (2000) 1563-1577
[4] N. Peters, Prog. Energy Combust. Sci. **10** (1984) 319-339
[5] N. Peters, Combust. Sci. Technol. **30** (1983) 1-17
[6] W.J. Pitz and C.J. Mueller, Prog. Energy Combust. Sci. **37** (2011) 330-350
[7] J. Abraham and L.M. Pickett, Atomization and Sprays **20** (2010) 241-250
[8] C. Bajaj, M. Ameem and J. Abraham, Combust. Sci. Technol. **185** (3) (2013) 454-472
[9] R. Seiser, H. Pitsch, K. Seshadri, W. Pitz and H. Gurran, Proc. Comb. Inst. **28** (2000) 2029-2037
[10] O. Herbinet, W.J. Pitz and C.K. Westbrook, Comb. Flame **154** (2008) 507-528
[11] Z. Luo, M. Plomer, T. Lu, S. Som, D.E. Longman, S. Sarthy and W.J. Pitz, Fuel **99** (2012) 143-153
[12] J. Appel, H. Bockhorn and M. Frenklach, Comb. Flame **121** (2000) 122-136
[13] M. Frenklach and J. Warnatz, Combust. Sci. Technol. **51** (1987) 265-283
[14] H. Wang and M. Frenklach, Journal Phy. Chem. **98** (1994) 11465-11489
[15] A. Kazakov and M. Frenklach, Comb. Flame **114** (1998) 484-501
[16] G.P. Smith, D.M. Golden, M. Frenklach, N.W. Moriarty, B. Eiteneer, M. Goldenberg, C.T. Bowman, R.K. Hanson, S. Song and W.C. Gardiner Jr., GRI-Mech 3.0 (1999)
[17] V. Gopalakrishnan, Modeling Combusting Diesel Jets: The Free Jet Regime, PhD Thesis, Purdue University, USA, 2003
[18] V. Gopalakrishnan and J. Abraham, Combust. Sci. & Technol. **176** (2004) 603-641
[19] S.R. Hoffman and J. Abraham, Fuel **88** (2009) 1099-1108